J Clust Sci (2017) 28:1319–1333
DOI 10.1007/s10876-016-1147-z

ORIGINAL PAPER

Green Synthesis of Silver Nanoparticles Using *Chenopodium aristatum L.* Stem Extract and Their Catalytic/Antibacterial Activities

Chun-Gang Yuan[1] · Can Huo[1] · Bing Gui[1] · Pengle Liu[1] · Cheng Zhang[2]

Received: 25 October 2016 / Published online: 24 December 2016

Abstract Compared with cultivated plants, wild weeds are cheaper and wider available for phytogenetic synthesis of nanoparticles. It is very valuable to distinguish the weed species from the local dominant wild plants for both efficient synthesis of nanoparticles and real industrial applications. In this study, a cheap, simple and novel biosynthesis method for silver nanoparticles (AgNPs) using *Chenopodium aristatum. L* stem extract as reducing and capping agents was developed. The real-time formation of AgNPs was monitored by UV–vis spectroscopy, and the SPR band was located at ~440 nm. The reaction factors including incubation time, $AgNO_3$ concentration, reaction temperature and pH were discussed and optimized. The synthesized AgNPs were quasi-spherical with the sizes from 3 to 36 nm. HRTEM images and XRD patterns showed that the AgNPs were with the face-centered cubic (fcc) structure. FTIR spectra indicated that some functional groups such like O–H, N–H, C–H, C=O were possibly responsible for reducing silver ions into nanoparticles and acted as capping agents to avoid agglomeration. The synthesized AgNPs exhibited strong catalytic activity in degradation of 4-nitrophenol and good antibacterial activity against *E. coli* and *S. aureus*. The proposed phytogenetic synthesis method is economical, simple and feasible.

Keywords Green synthesis · Silver nanoparticles · *Chenopodium aristatum. L* extract · Catalytic and antibacterial activities

✉ Chun-Gang Yuan
chungangyuan@hotmail.com

[1] School of Environmental Science & Engineering, North China Electric Power University, Baoding 071000, China

[2] State Key Laboratory of Coal Combustion, Huazhong University of Science and Technology, Wuhan 430074, China

Introduction

Silver nanomaterials (or silver nanoparticles, AgNPs) have been applied in many fields (such as food technology, cosmetics and medical products, textiles/fabrics, semiconductor and optical devices), which leads to a growing demand in recent years [1–4]. However, the wide utilization of silver nanomaterials can potentially cause at least two adverse effects on our environment. The first one is the unavoidable involvement of toxic chemicals during its synthesis process. The second one is the direct toxicity of nanoparticles to biota when they are released into the environment during/after use. Therefore, it is an import mission for the researchers all over the world to hunt green and benign methods for synthesis of nanoparticles [5]. More biocompatible and safer nano-products are expected for the sustainable nanoscience and technology in the future [6]. Biogenetic synthesis of AgNPs using microbe or plant extract has received significant attentions because both the procedures and the products are much more benign and biocompatible compared with physical/chemical methods [7–9]. Among these biogenetic methods, plant mediated synthesis is regarded as the most feasible technique for real industrial amplification with low cost, easiness and simplicity [10, 11]. In recent years, biosynthesis methods of nanoparticles using plants or plant extracts have been widely studied and applied [12–21]. Various tissues of plants were used to prepare AgNPs including leaves [21–32], pods [12], seeds [13, 33, 34], peel and rind [14, 35], fruit [15, 36], rhizome [16], roots [37], bark [17, 38, 39] and tuber [18]. By regulating the experimental conditions, AgNPs with various morphologies can even be obtained [40–46]. Ahmed et al. [2] reviewed on plants extract mediated synthesis of silver nanoparticles for antimicrobial applications. Dauthal and Mukhopadhyay [9] gave us a detailed discussion about plant-mediated synthesis, mechanistic aspects of synthesis, and applications of noble metals nanoparticles. Qazi et al. [47] also reviewed biogenetic synthesis of nanoparticles very recently. These critical reviews not only summarized the present literatures but also highlighted the potential of this field to open up new avenues for researchers [47]. They indicated that biogenetic synthesis of nanoparticles was a promising and practical strategy for the sustainable development of nanoscience and technology in the coming decades [2, 9, 47].

From the both economic and scientific points, it is very valuable and significant to use wild species (or weeds) for phytogenetic synthesis instead of the cultivated one. Compared with other cultivated plants (such like vegetables, fruits or flowers), wild weeds always spontaneously grow in the open fields or on hills and the cost to use wild weeds for biosynthesis can become much cheaper. Low cost and easy availability of the resource plants can make the phytogenetic synthesis method practical for real applications. It will be very exciting and significant if we are able to distinguish the effective species from the local dominant wild species for the efficient synthesis of nanoparticles.

Chenopodium aristatum. L (*C. aristatum. L*) is one of the members of *Chenopodiaceae* family and universally distributed in north of China (as well as other countries at the similar latitude), especially in Hebei province. It is an annual

herb that grows in fields and slopes as an obnoxious weed. This dominant weed grows fast and can provide an enormous amount of biomass every year, which can potentially supply us plenitudinous and cheap resources for phytogenetic synthesis. It is well known that the plants belonging to *Chenopodium* are rich of flavonoids (mainly kaempferol and quercetin glucosides), phenolic acids and terpenoids. These bioactive compounds have been regarded as effective reducing agents for biosynthesis of nanoparticles. Based on this, we believe that *C. aristatum. L* should be able to act as a new, powerful and economic wild species to biosynthesize silver nanoparticles in our local region.

To the best of our knowledge, this study should be the first report about the green synthesis of silver nanoparticles using *C. aristatum. L.* The synthesis process of AgNPs was monitored and studied by UV–vis spectroscopy. The morphology and structure of AgNPs were measured by transmission electron microscopy (TEM) and X-ray diffraction (XRD). Fourier transform infrared (FTIR) was applied to confirm the functional groups which were possibly responsible for reducing silver ions and stabilizing AgNPs. The catalytic activity of the AgNPs was studied by the degradation of 4-nitrophenol, and the antibacterial activity was tested by inhibition against *E. coil* and *S. aureus.*

Materials and Methods

Materials

C. aristatum. L was harvested and collected in local roadsides in Baoding city and entirely washed with deionized water. The stem of *C. aristatum. L.* was carefully cut into species (2–3 cm in length) with a knife and dried in air. The dried stems were ground to powder and sieved with a 100 mesh sieve for the preparation of the extract. Silver nitrate, 4-nitrophenol, sodium borohydride, and sodium hydroxide were purchased from Kermel Chemical Reagent (Tianjin, China). All glassware was washed by concentrated HNO_3 and deionized water.

Synthesis of AgNPs

1.0 g of *C. aristatum. L* stem powder was added to 100 mL deionized water and boiled at 100 °C for 10 min. The extract was filtered through 100 nm membrane after cooling down. 400 μL of $AgNO_3$ solution (100 mM) was added to 9.6 mL of the extract to keep the concentration of $AgNO_3$ at 4 mM in the final mixed solution. The production of AgNPs was confirmed by a color change of the mixture from light greenish-yellow to brown.

Characterization of AgNPs

The formed AgNPs were monitored by a UV–visible spectrophotometer (Pgeneral, China) with a resolution of 1 nm in a wavelength range of 300–800 nm. The yields of AgNPs synthesized by both phytogenetic and chemical method were determined

by inductively coupled plasma-mass spectrometry (Agilent 7500 ce, USA). In this experiment, the plant extract was replaced by trisodium citrate dihydrate solution (34 mM), which was used as the chemical reduction reagent to synthesize AgNPs in the mixture. The colloid was filtered by an ultrafiltration tube (Amicon Ultra-15, 3 KD, Millipore, MA) at 9600 rpm for 40 min when the reaction finished (the same time span as the phytogenetic method). The concentration of silver in the filtrate was determined by ICP-MS, and represented the amount of unreacted Ag^+ in the mixture. The yields of the reactions were calculated by comparing the amount of the reacted Ag^+ with the original amount of Ag^+ ($AgNO_3$). The size and morphology were characterized by transmission electron microscopy (Tecnai G^2 F20 S-TWIN, FEI/America). The crystal structure of the AgNPs was analyzed by X-ray powder diffractometer (D8 ADVANCE, Bruker/Switzerland). Fourier transform infrared spectroscopy (Magna-IR 750/America) analysis was applied to identify the biomolecules which were possibly responsible for the reduction of Ag^+ and stabilization of nanoparticles.

Catalytic Activity

The catalytic activity of the synthesized AgNPs was investigated by degradation of 4-nitrophenol in the presence of $NaBH_4$. A typical experimental procedure was carried out as following: 200 μL of freshly prepared $NaBH_4$ (5 M) and 20 μL of 4-nitrophenol (4-NP, 20 mM) were added into a standard quartz cell and mixed with 2760 μL of the sterile DI water. 20 μL of AgNPs colloid was then added into the mixture, and the reaction process was monitored by UV–vis spectroscopy.

Antibacterial Activity

Antibacterial activity of AgNPs was tested by the oxford cup method. *S. aureus* and *E. coli* were grown on LB medium at 37 °C for 18 h, respectively. The culture were then pipetted into the solid LB medium and evenly smeared. Five oxford cups were placed on the surface of the solid LB medium. 50 μL of *C. aristatum. L* stem extract, AgNPs (1, 2 and 4 mM), and gentamicin(4 μg/mL, positive control) were injected into oxford cup, respectively. The petri-dishes were incubated at 37 °C for 24 h. After culture, the zones of inhibition were measured. Three replicates were tested for each bacteria strain.

Result and Discussion

Visual Observation and UV–vis Spectral Studies

The formation of AgNPs was observed by a color change from light greenish-yellow to brown due to the excitation of the surface plasmon resonance (SPR) [48]. Figure 1 shows the visual observations of the reaction mixture under various $AgNO_3$ concentrations with the constant extract volume, pH, and temperature. The color of the AgNPs colloid changed from light brown to reddish brown with $AgNO_3$

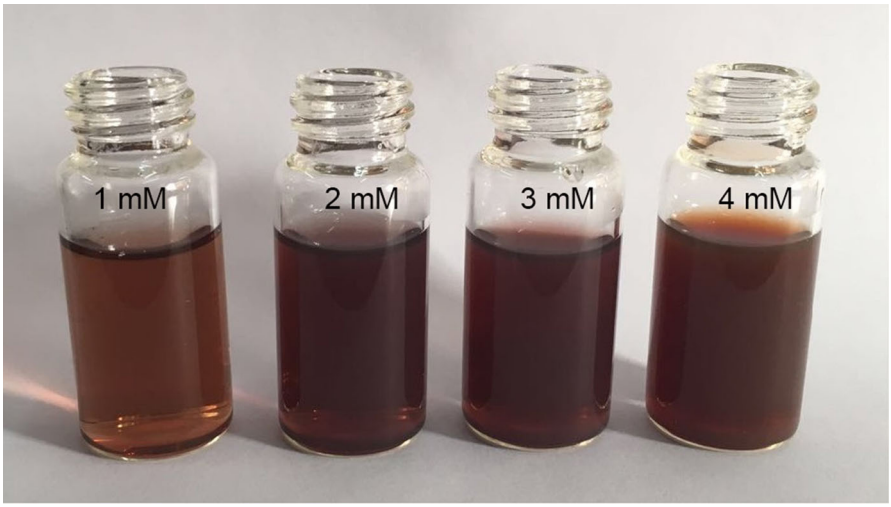

Fig. 1 Visual observations of reaction mixture at various $AgNO_3$ concentrations

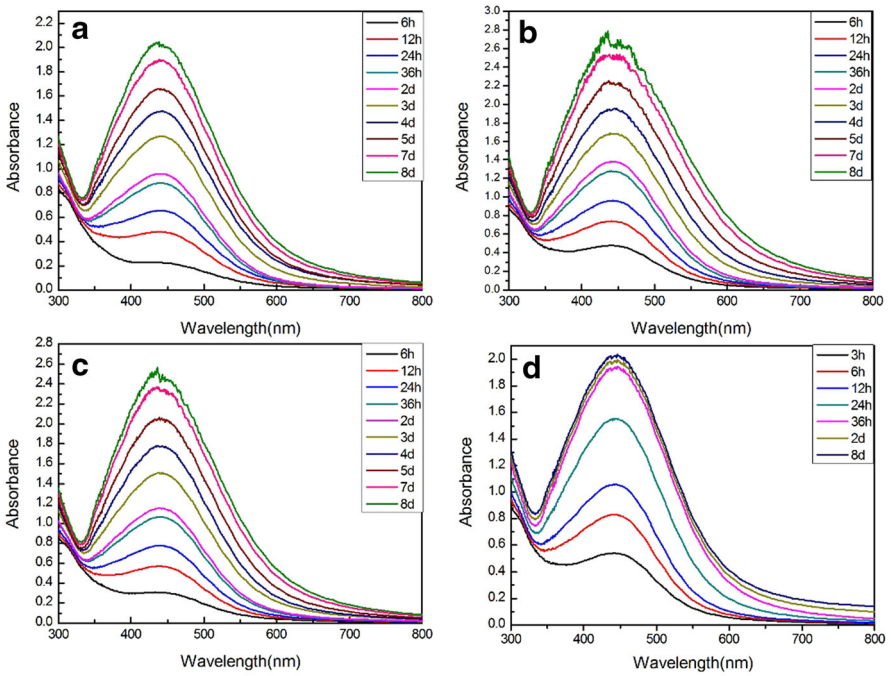

Fig. 2 The spectra of synthesized AgNPs at different $AgNO_3$ concentrations **a** 1 mM, **b** 2 mM, **c** 3 mM, **d** 4 mM

concentration increasing. Figure 2 demonstrates the UV–vis spectra of AgNPs prepared under various $AgNO_3$ concentrations. It is observed that the SPR band for each $AgNO_3$ concentration doesn't shift, which indicates that the synthesized

AgNPs had good stabilities. Varying the $AgNO_3$ concentration from 1 to 4 mM led to a slight red shift of SPR band from 442 to 446 nm. The red shift revealed the formation of bigger AgNPs at higher $AgNO_3$ concentration. For each sample, the intensity of SPR band can be enhanced, and more AgNPs will be prepared with reaction time. ICP-MS measurement showed that almost 78.2% of the total Ag^+ had been converted into the AgNPs during the process. Although the yield of the phytogenetic method was lower than that of the chemical method (95.8%), the phytogenetic method is more environmental friendly and cost effective [49].

The pH of extract usually plays a crucial role in the synthesis of AgNPs. In our study, the extract pH values (2, 4, 6, 8, 10, 11, and 12) were adjusted by adding diluted HNO_3 (0.1 M) or NaOH (0.1 M) solution. 400 μL of $AgNO_3$ solution (100 mM) was added to 9.6 mL treated extract to start the biosynthesis procedure. The intensity of peak was much stronger, and the peak was sharper under higher pH conditions with the same incubation time. There was no significant peak observed under acidic conditions (Fig. 3). It may owe to the electrostatic repulsion of anions present in alkaline solution to prohibit aggregation of the formed AgNPs [50]. A strong and sharp peak (pH = 12) was observed at 414 nm, which revealed that the bursting formation of AgNPs in solution under strong alkaline conditions [51]. The SPR band shifted from 414 to 425 nm with pH decreasing (from 12 to 8) due to the AgNPs size enlarging. From our results, the sizes and shapes of AgNPs can be regulated by controlling the pH of the reaction solution.

Temperature is one of the critical parameters that influence the stability, activity and chemical characters of nanoparticles, as well as the reaction speed [52]. The effects of the reaction temperature on the synthesis of AgNPs are showed in Fig. 4. It is observed that the reaction speed can be dramatically promoted by increasing temperature (Fig. 4A). A significant absorption peak rapidly appeared only after

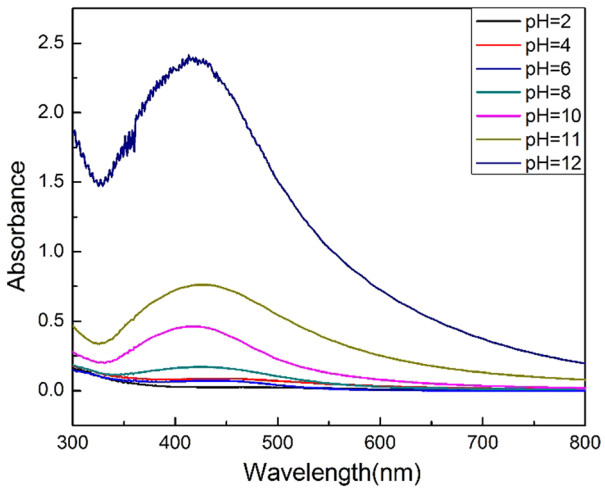

Fig. 3 The spectra of synthesized AgNPs under different pH

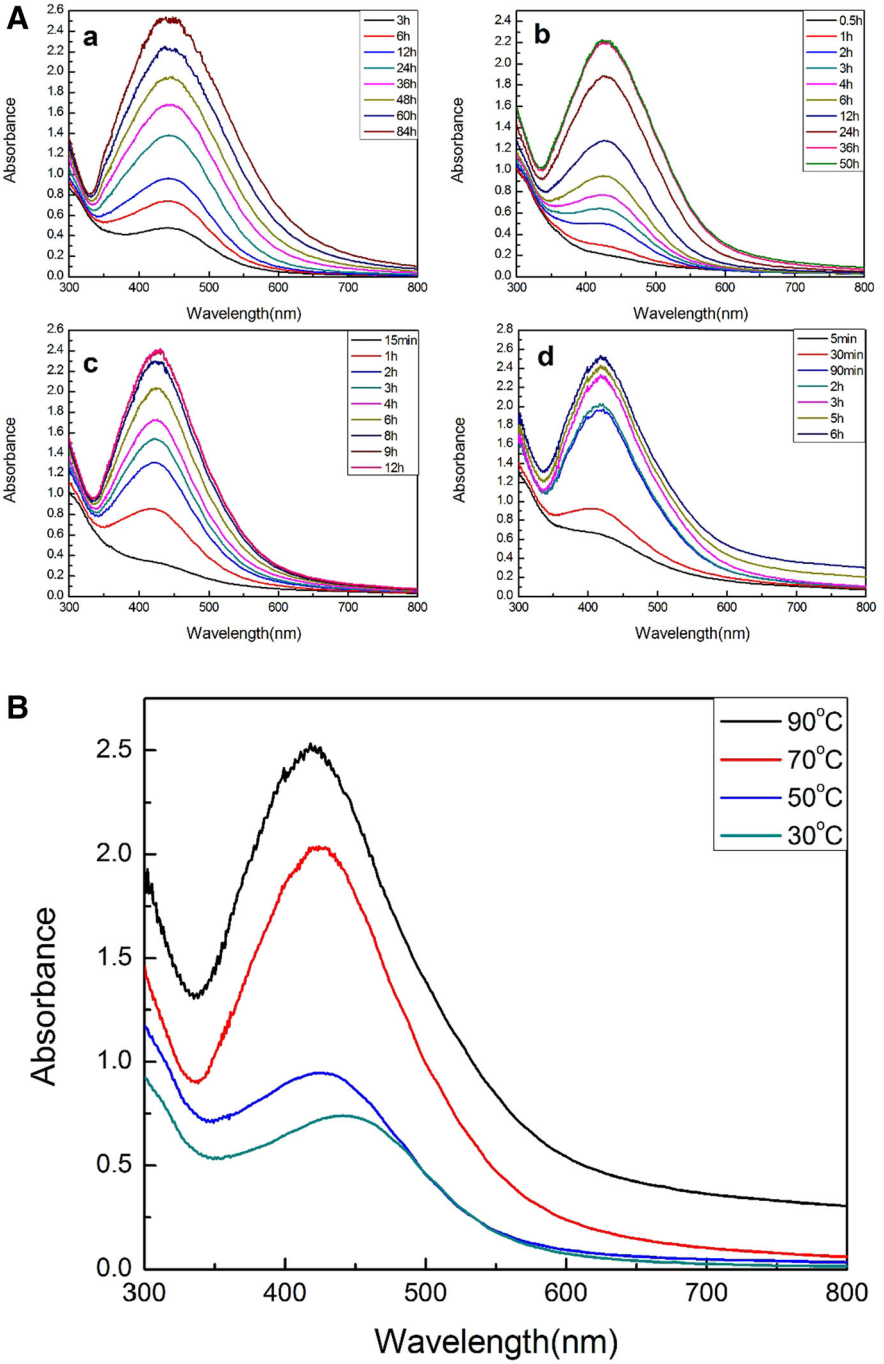

Fig. 4 **A** UV–vis spectra of synthesized AgNPs at different temperatures (*a*) 30 °C, (*b*) 50 °C, (*c*) 70 °C, (*d*) 90 °C. **B** UV–Vis spectra of AgNPs at different temperatures (6 h reaction)

5 min reaction at 90 °C. Figure 4B shows the effect of temperature on the wavelength shift of the AgNPs. The blue shift of the SPR band can be observed with temperature increasing, which indicated the AgNPs with smaller sizes can be obtained at a higher temperature. We speculate that more silver ions can be reduced to Ag^0 rapidly at a higher temperature and the reduced Ag^0 atoms can be readily aggregated to form a new cluster. The formed cluster can act as anucleation to continuously absorb Ag^0 in solution to grow into nanoparticles. The bioactive compounds in solution can cap and stabilize the as-formed nanoparticles immediately, and a large number of maller particles can be obtained. The strong and narrow absorption peak at a higher temperature also indicates that the AgNPs synthesized at high temperature have a narrow particle size distribution and they are stable in solution (Fig. 4B).

TEM and EDS Analysis

TEM images (Fig. 5a) demonstrate the shapes of synthesized AgNPs are predominant quasi-spherical with a size range of 3–36 nm, and most of the particles are about 14 nm. The AgNPs are surrounded by a thin and transparent layer of organic material which was responsible for enhancing the stability of prepared AgNPs. Figure 5b shows the clear and regular lattice fringes of 0.23 nm that correspond to (111) lattice plane of face-centered cubic (fcc) structure of AgNPs. The corresponding fast Fourier transform (FFT) image (Fig. 5c) also confirms the crystalline pattern of the synthesized AgNPs.

The EDS spectra of the AgNPs are showed in Fig. 6a. A strong signal of metallic silver is clearly observed. A signal of potassium is also present for the provenience of K in the original *C. aristatum. L* stem extract. Figure 6b displayed the elemental mapping of the synthesized AgNPs, which reveals that K element surrounded elemental Ag^0.

XRD Analysis

XRD was used to confirm the crystal structure of the synthesized nanoparticles. Figure 7 shows that the diffraction peaks are at 38.18°, 44.29°, 64.43°, 77.48°, 81.54° which corresponds to (111), (200), (220), (311) and (222) planes of face-centered cubic silver [24, 26, 27, 37, 39]. The patterns show good match with the JCPDS file No. 087-0717 [33, 37]. The XRD analysis demonstrates that the synthesized AgNPs using *C. aristatum. L.* stem extract is crystalline in nature. The mean size of AgNPs calculated by Debye–Scherrer's equation is about 16 nm, which is in agreement with the result of TEM analysis.

FTIR Analysis

FTIR is often used to study the biomolecules in plant extract which are possibly responsible for the synthesis of nanoparticles. The spectra have no significant

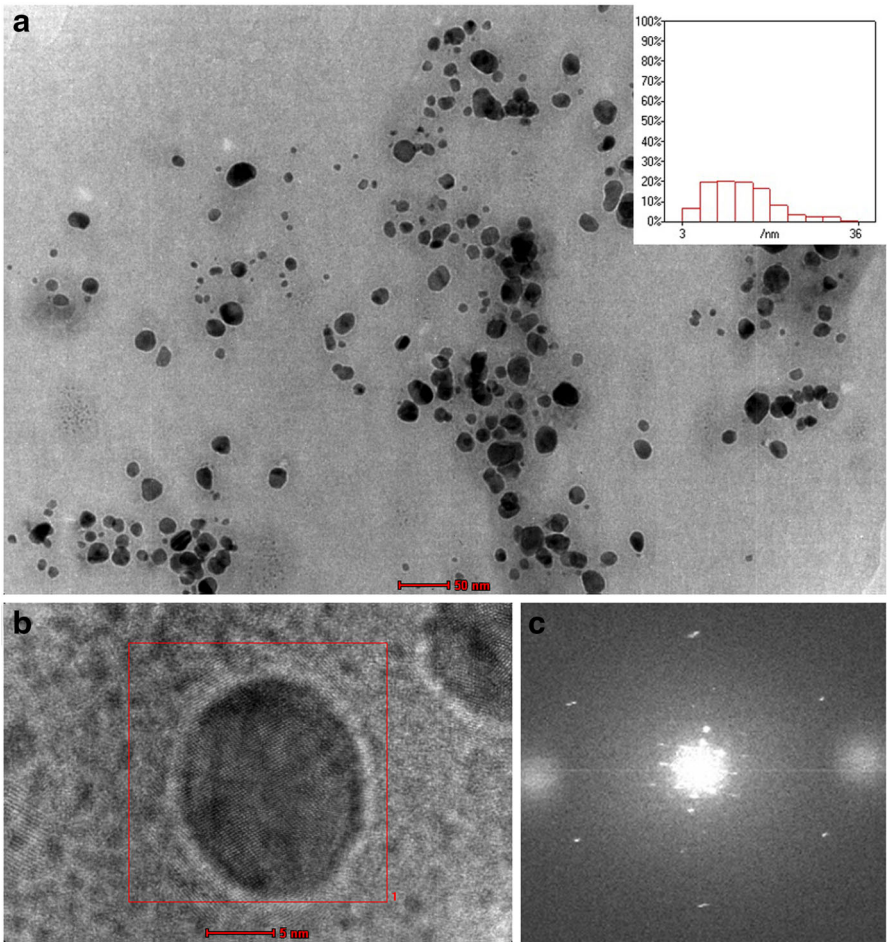

Fig. 5 **a** TEM micrograph of synthesized AgNPs (*inset* shows size distribution *histogram*), **b** HRTEM micrograph of synthesized AgNPs, **c** FFT pattern

change between *C. aristatum. L.* stem extract and the synthesized AgNPs (Fig. 8). The peak at 3412 cm^{-1} is related to the stretching vibration for O–H of phenols and carboxylic acids [35] or N–H vibrational frequency [31]. The peak at 2921 cm^{-1} is assigned to the symmetric and asymmetric C–H stretching vibration [24]. The sharp absorption peak at 1630 cm^{-1} can be the N–H stretching of the primary amines and the C=O bond of the carbonyl group also appears in this range [30, 36]. The band at 1625 cm^{-1} was assigned to C=C stretching vibration of the phytoconstituents [35, 39]. The band at 1050 cm^{-1} was due to the vibrations of –C–O group of constituents [34, 39]. The peak at 616 cm^{-1} may be assigned to the δ(C–H) bending vibrations or C–S, R–C–CH_3 stretching for sulfur compounds [34, 38]. It infers that biomolecules like flavonoids and alkaloids are responsible for reducing Ag^{+} to Ag^{0} and stabilizing the synthesized nanoparticles.

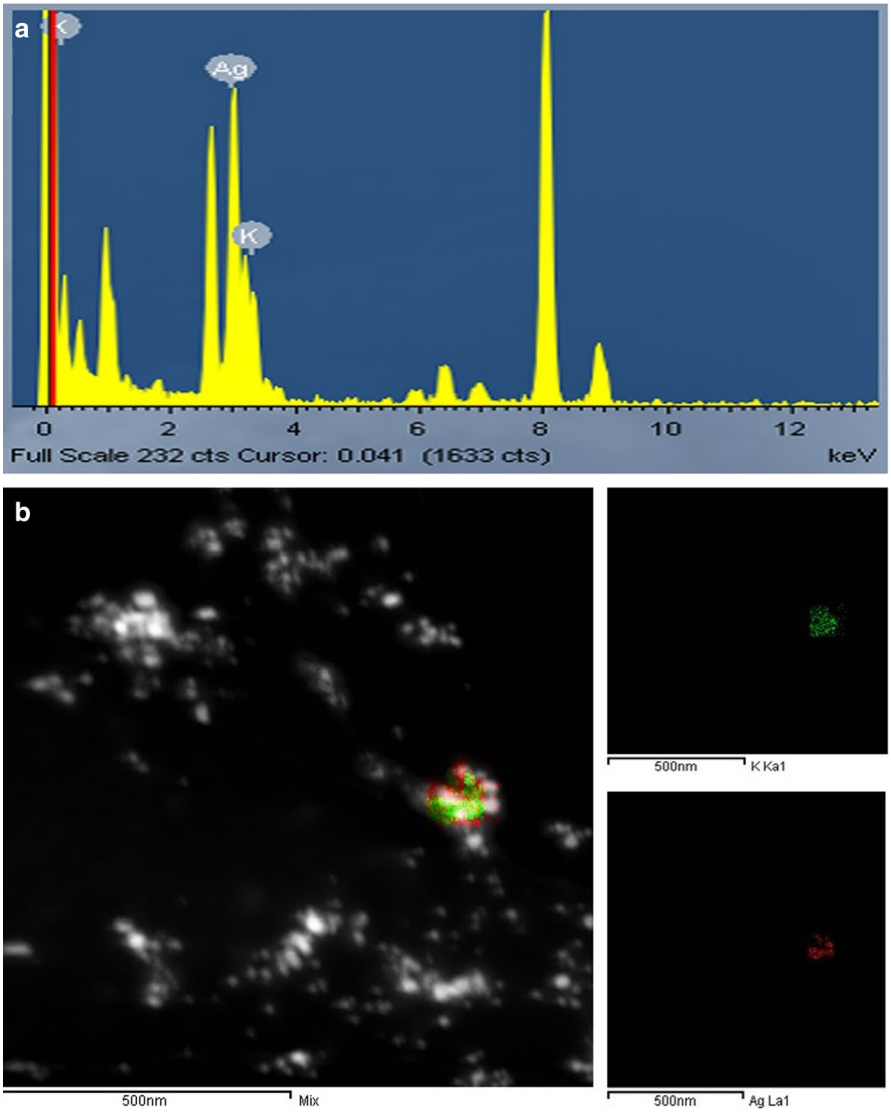

Fig. 6 **a** EDS analysis of synthesized AgNPs, **b** selected area elemental mapping of synthesized AgNPs using *C. aristatum. L.* stem extract

Catalytic Activity

In this study, the catalytic activity of AgNPs synthesized at different temperatures was demonstrated by degradation of 4-NP to 4-AP in the presence of $NaBH_4$ (Fig. 9). The mixture of 4-NP and $NaBH_4$ has the λ_{max} at 400 nm due to the formation of 4-nitrophenolate ions [53]. After the addition of the AgNPs, the intensity of the 4-nitrophenolate ions peaks decreased and new peaks appeared at

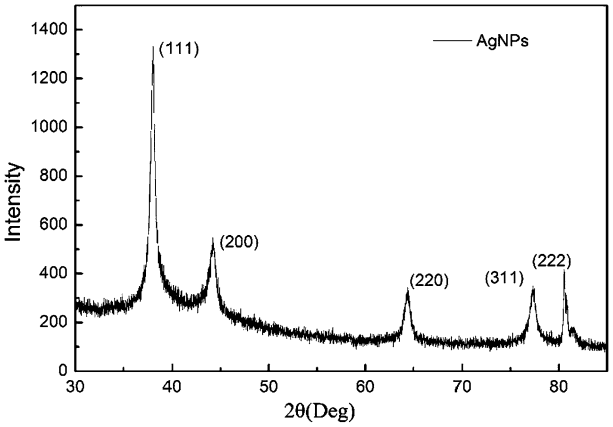

Fig. 7 XRD patterns of the synthesized AgNPs

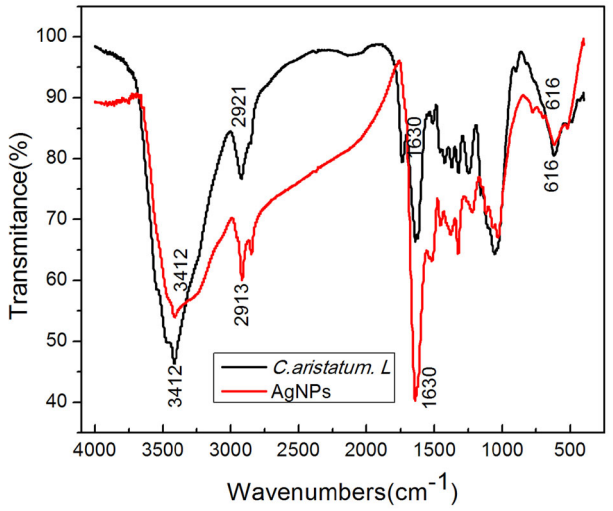

Fig. 8 FTIR spectra of *C. aristatum. L. stem* and the synthesized AgNPs

313 nm, which indicated the formation of 4-AP. 10 min later, the peaks at 400 nm were disappeared and the color of reactant changed from yellow to colorless, which means the accomplishment of the reaction. Furthermore, synthesis temperature has no significant influences on the degradation rate of 4-NP, due to light difference of the AgNPs synthesis at different temperature. The reaction time was slightly shortened to 10 min from 14 min with the elevated synthesis temperature.

The degradation kinetics of the reaction system can be calculated by the Langmuir and Hinshelwood model by the relationship between the rate of the degradation of 4-NP in the presence of AgNPs with respect to time [54]. Because the concentration of $NaBH_4$ was large enough compared with the concentration of 4-NP. Hence, the reaction rate (Ka) was only assumed to be dependent of the

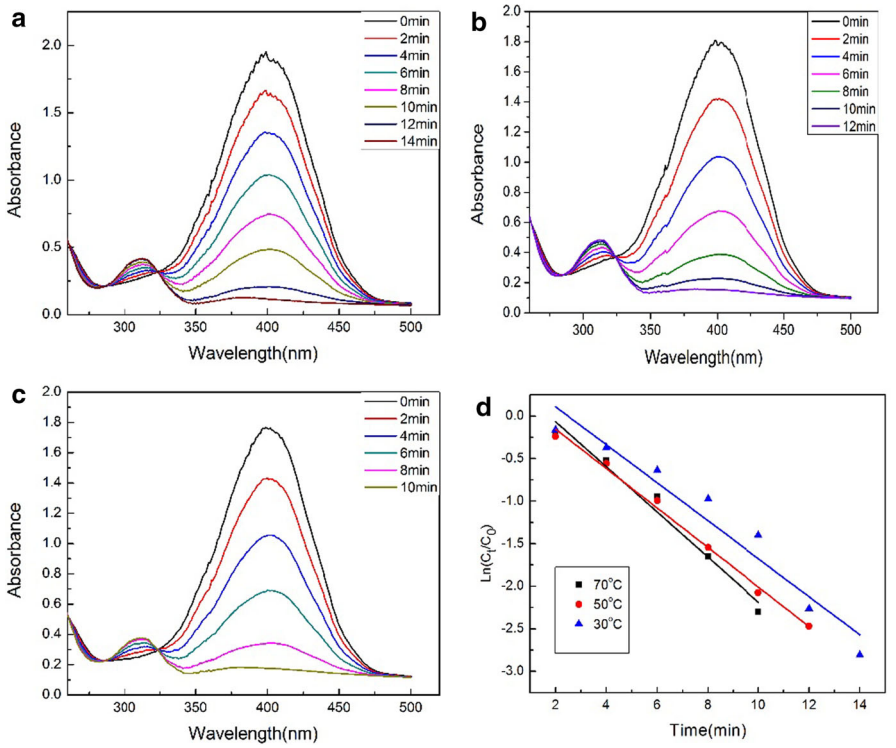

Fig. 9 Catalytic activity of the AgNPs synthesized at different temperatures. **a** 30 °C, **b** 50 °C, **c** 70 °C, **d** the logarithm of the ratio between its final concentration and the initial concentration of 4-NP versus corresponding time

concentration of the 4-NP. The rate of equation can be simplified and integrated to be:

$$\mathrm{Kat} = \ln(C_t/C_0) = \ln(A_t/A_0)$$

where C_0 and A_0 are the initial concentration and absorption of reactants, while C_t and A_t are the concentration and absorption of reactant at any time t.

Plotting $\ln(C_t/C_0)$ versus the corresponding time (min) showed linear relationship in Fig. 9d. The rate constants (k) for the degradation of 4-NP using AgNPs synthesized at different temperatures were found to be 0.2232, 0.2320 and 0.2653 min^{-1}, respectively. The synthesized AgNPs performs strong catalytic activities.

Antibacterial Activity

In our study, the synthesized AgNPs showed the effective antibacterial activity against both gram negative (*E. coli*) and gram positive (*S. aureus*) bacterium, and these two bacteria were not susceptible to *C. aristatum. L.* stem extract (Fig. 10). It was found that the inhibition zones were dose dependent with AgNPs concentration.

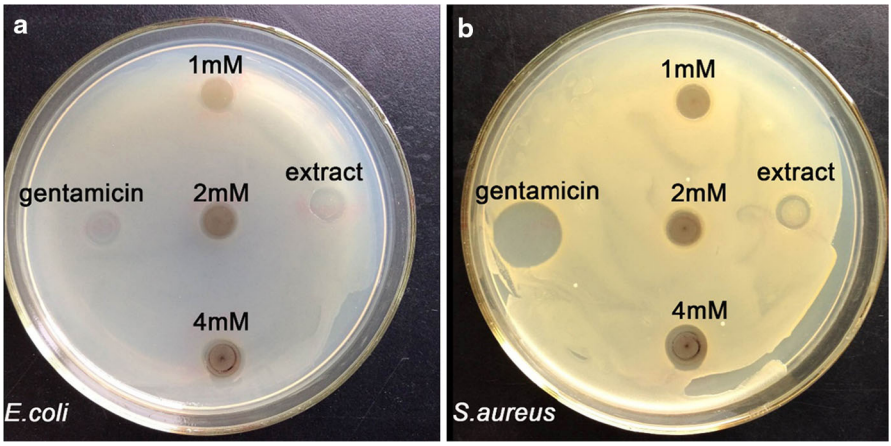

Fig. 10 Antibacterial activity of the synthesized AgNPs against *E. coli* (**a**) and *Saureus* (**b**)

Conclusion

A phytogenetic synthesis method for AgNPs using *Chenopodium aristatum. L.* stem extract was developed. In this study, the synthesized AgNPs were predominantly quasi-spherical with a size range of 3–26 nm and most of them were 14 nm. HRTEM images and XRD patterns demonstrated that the AgNPs were in the face-centered cubic (fcc) structure. The synthesized AgNPs showed good catalytic and antibacterial activities. Compared with other cultivated plants, *Chenopodium aristatum. L.* always spontaneously grows in the open country or wilderness with a large biomass production. The easy availability of *Chenopodium aristatum. L.* and the fast growth rate of AgNPs enable the whole synthesis procedure cost effective and feasible for real applications.

Acknowledgements This work was kindly co-funded by the National Natural Science Foundation of China (21277043, 21620102008), the Beijing Natural Science Foundation (8132038), the Foundation of State Key Laboratory of Coal Combustion (FSKLCC1414) and the Fundamental Research Funds for the Central Universities.

References

1. Q. Chaudhry and L. Castle (2011). *Trends. Food. Sci. Tech.* **22**, 595–603.
2. S. Ahmed, M. Ahmad, B. L. Swami, and S. Ikram (2016). *J. Adv. Res.* **7**, 17–28.
3. G. Martínez-Castañón, F. Martínez-Gutierrez, J. Martínez-Mendoza, and F. Ruiz (2008). *J. Nanopart. Res.* **10**, 1343–1348.
4. C. Larue, H. Castillo-Michel, S. Sobanska, L. Cécillon, S. Bureau, V. Barthès, L. Ouerdane, M. Carrière, and G. Sarret (2014). *J. Hazard. Mater.* **264C**, 98–106.
5. P. Singh, Y. J. Kim, D. Zhang, and D. C. Yang (2016). *Trends. Biotechnol.* **34**, 588–599.
6. R. Rajan, K. Chandran, S. L. Harper, S. I. Yun, and P. T. Kalaichelvan (2015). *Ind. Crop. Prod.* **70**, 356–373.
7. M. Apte, P. Chaudhari, A. Vaidya, A. R. Kumar, and S. Zinjarde (2016). *Colloid Surf.* **A501**, 1–8.
8. S. A. Annu, S. Ikram, and Y. S. Salprima (2016). *J. Phototoch. Photobio. B* **161**, 141–153.
9. P. Dauthal and M. Mukhopadhyay (2016). *Ind. Eng. Chem. Res.* **55**, 9557–9577.

10. I. M. Chung, I. Park, K. Seunghyun, M. Thiruvengadam, and G. Rajakumar (2016). *Nanoscale. Res. Lett.* **11**, 1–14.
11. K. Kalishwaralal, V. Deepak, S. B. R. K. Pandian, M. Kottaisamy, S. Barathmanikanth, B. Kartikeyan, and S. Gurunathan (2010). *Colloid Surf. B* **77**, 257–262.
12. P. Nalawade, P. Mukherjee, and S. Kapoor (2014). *Spectrochim. Acta. A* **129C**, 121–124.
13. U. B. Jagtap and V. A. Bapat (2013). *Ind. Crop. Prod.* **46**, 132–137.
14. S. Kaviya, J. Santhanalakshmi, B. Viswanathan, J. Muthumary, and K. Srinivasan (2011). *Spectrochim. Acta. A* **79**, 594–598.
15. M. Ghaffari-Moghaddam and R. Hadi-Dabanlou (2014). *J. Ind. Eng. Chem.* **20**, 739–744.
16. P. P. N. V. Kumar, S. V. N. Pammi, P. Kollu, K. V. V. Satyanarayana, and U. Shameem (2014). *Ind. Crop. Prod.* **52**, 562–566.
17. M. Sathishkumar, K. Sneha, I. S. Kwak, J. Mao, S. J. Tripathy, and Y. S. Yun (2009). *J. Hazard. Mater.* **171**, 400–404.
18. S. Ghosh, S. Patil, M. Ahire, R. Kitture, A. Jabgunde, S. Kale, K. Pardesi, J. Bellare, D. D. Dhavale, and B. A. Chopade (2011). *J. Nanomater.* **2011**, 18083–18088.
19. D. Philip and C. Unni (2011). *Physica E* **43**, 1318–1322.
20. M. M. H. Khalil, E. H. Ismail, and F. El-Magdoub (2012). *Arab. J. Chem.* **5**, 431–437.
21. D. Philip (2010). *Physica E* **42**, 1417–1424.
22. A. Nabikhan, K. Kandasamy, A. Raj, and N. M. Alikunhi (2010). *Colloid Surf.* **B79**, 488–493.
23. C. S. Espenti, K. S. V. K. Rao, and K. M. Rao (2016). *Mater. Lett.* **174**, 129–133.
24. J. L. López-Miranda, M. Vázquez, N. Fletes, R. Esparza, and G. Rosas (2016). *Mater. Lett.* **176**, 285–289.
25. A. Verma and M. S. Mehata (2015). *J. Radiat. Res. Appl. Sci.* **9**, 109–115.
26. V. Ravichandran, S. Vasanthi, S. Shalini, S. A. A. Shah, and R. Harish (2016). *Mater. Lett.* **180**, 264–267.
27. M. J. Ahmed, G. Murtaza, A. Mehmood, and T. M. Bhatti (2015). *Mater. Lett.* **153**, 10–13.
28. S. Ahmed, S. Ullah, M. Ahmad, B. L. Swami, and S. Ikram (2016). *J. Radiat. Res. Appl. Sci.* **9**, 1–7.
29. B. Paul, B. Bhuyan, D. D. Purkayastha, and S. S. Dhar (2016). *J. Phototoch Photobio. B* **154**, 1–7.
30. N. Khatoon, R. Ahmad, and M. Sardar (2015). *Biochem. Eng. J.* **102**, 91–97.
31. M. A. Farah, M. A. Ali, S. M. Chen, Y. Li, F. M. Al-Hemaid, F. M. Abou-Tarboush, K. M. Al-Anazi, and J. Lee (2016). *Colloid Surf. B* **141**, 158–169.
32. R. A. Morales-Luckie, A. A. Lopezfuentes-Ruiz, O. F. Olea-Mejía, A. F. Liliana, V. Sanchez-Mendieta, W. Brostow, and J. P. Hinestroza (2016). *Mater. Sci. Eng. C* **69**, 429–436.
33. V. Dhand, L. Soumya, S. Bharadwaj, S. Chakra, D. Bhatt, and B. Sreedhar (2016). *Mater. Sci. Eng. C* **58**, 36–43.
34. S. Mohammadi and S. Pourseyedi (2016). *J. Environ. Chem. Eng.* **4**, 2023–2032.
35. J. K. Patra, G. Das, and K. H. Baek (2016). *J. Phototoch. Photobio. B* **161**, 200–210.
36. B. Kumar, K. Smita, L. Cumbal, J. Camacho, E. Hernández-Gallegos, M. Grijalva, and K. Andrade (2016). *Mater. Sci. Eng. C* **62**, 725–731.
37. N. H. Rao, N. Lakshmidevi, S. V. N. Pammi, P. Kollu, S. Ganapaty, and P. Lakshmi (2016). *Mater. Sci. Eng. C* **62**, 553–557.
38. D. Nayak, S. Ashe, P. R. Rauta, M. Kumari, and B. Nayak (2016). *Mater. Sci. Eng. C* **58**, 44–52.
39. T. N. Edison, Y. R. Lee, and M. G. Sethuraman (2016). *Spectrochim. Acta. A* **161**, 122–129.
40. C. Krishnaraj, E. G. Jagan, S. Rajasekar, P. Selvakumar, P. T. Kalaichelvan, and N. Mohan (2010). *Colloid Surf. B* **76**, 50–56.
41. H. Alishah, S. P. Seyedi, S. Y. Ebrahimipour, and S. Esmaeili-Mahani (2016). *J. Clust. Sci.* **27**, 421–429.
42. T. N. J. I. Edison, E. R. Baral, Y. R. Lee, and S. H. Kim (2016). *J. Clust. Sci.* **27**, 285–298.
43. S. C. Bankalgi, R. L. Londonkar, U. Madire, and N. K. A. Tukappa (2016). *J. Clust. Sci.* **27**, 1485–1497.
44. M. Khatami, R. Mehnipor, M. H. S. Poor, and G. S. Jouzani (2016). *J. Clust. Sci.* **27**, 1601–1612.
45. J. Venugobal and K. Anandalakshmi (2016). *J. Clust. Sci.* **27**, 1683–1699.
46. Y. G. Yin, X. Y. Yang, L. G. Hu, Z. Q. Tan, L. X. Zhao, Z. Zhang, J. F. Liu, and G. B. Jiang (2016). *Environ. Sci. Technol. Lett.* **3**, (4), 160–165.
47. F. Qazi, Z. Hussain, and M. N. Tahir (2016). *RSC Adv.* **6**, 60277–60286.
48. S. S. Shankar, A. Ahmad, R. Pasricha, M. I. Khan, R. Kumar, and M. Sastry (2004). *J. Colloid. Inter. Sci.* **274**, 69–75.
49. S. J. Yu, Y. G. Yin, X. X. Zhou, L. J. Dong, and J. F. Liu (2016). *Environ. Sci Nano.* **3**, 883–893.

50. A. Tripathy, A. M. Raichur, N. Chandrasekaran, and T. C. Prathna (2010). *J. Nanopart. Res.* **12**, 237–246.
51. M. Ahamed, M. A. M. Khan, M. K. J. Siddiqui, M. S. Alsalhi, and S. A. Alrokayan (2011). *Physica E* **43**, 1266–1271.
52. S. Link and M. A. El-Sayed (1999). *J. Phys. Chem. B* **103**, 4212–4217.
53. N. Muniyappan and N. S. Nagarajan (2014). *Process Biochem* **49**, 1054–1061.
54. C. Tamuly, M. Hazarika, M. Bordoloi, P. K. Bhattacharyya, and R. Kar (2014). *Spectrochim. Acta A* **132**, 687–691.